The Astrophysical Journal, 631:1022–1031, 2005 October 1

AFTERGLOW LIGHT CURVES FROM IMPULSIVE RELATIVISTIC JETS WITH AN UNCONVENTIONAL STRUCTURE

Jonathan Granot
Kavli Institute for Particle Astrophysics and Cosmology, Stanford University, P.O. Box 20450, MS 29, Stanford, CA 94309; granot@slac.stanford.edu
Received 2005 April 12; accepted 2005 June 13

ABSTRACT

The jet structure in gamma-ray burst (GRB) sources is still largely an open question. The leading models invoke either (1) a roughly uniform jet with sharp edges or (2) a jet with a narrow core and wide wings where the energy per solid angle drops as a power law with the angle θ from the jet symmetry axis. Recently, a two-component jet model has also been considered, with a narrow uniform jet of initial Lorentz factor $\Gamma_0 \gtrsim 100$ surrounded by a wider uniform jet with $\Gamma_0 \sim 10-30$. Some models predict more exotic jet profiles, such as a thin uniform ring (i.e., the outflow is bounded by two concentric cones of half-opening angle θ_c and $\theta_c + \Delta\theta$, with $\Delta\theta \ll \theta_c$) or a fan (a thin outflow with $\Delta\theta \ll 1$ along the rotational equator, $\theta_c = \pi/2 + \Delta\theta/2$). In this paper we calculate the expected afterglow light curves from such jet structures, using a simple formalism that is developed here for this purpose and could also have other applications. These light curves are qualitatively compared to observations of GRB afterglows. It is shown that the two-component jet model cannot produce very sharp features in the afterglow light curve due to the deceleration of the wide jet or the narrow jet becoming visible at lines of sight outside the edge of the jet. We find that a "ring"-shaped jet or a "fan"-shaped jet produces a jet break in the afterglow light curve that is too shallow compared to observations, where the change in the temporal decay index across the jet break is about half of that for a uniform conical jet. For a ring jet, the jet break is divided into two distinct and smaller breaks, the first occurring when $\gamma\Delta\theta \sim 1-2$ and the second when $\gamma\theta_c \sim \frac{1}{2}$.

Subject headings: gamma rays: bursts — gamma rays: theory — ISM: jets and outflows — radiation mechanisms: nonthermal — relativity

Online material: color figures

1. INTRODUCTION

Different lines of evidence suggest that GRB outflows are collimated into narrow jets. An indirect but compelling argument comes from the very high values for the energy output in gamma rays assuming isotropic emission, $E_{\gamma,\rm iso}$, that are inferred for GRBs with known redshifts, z, which approach and in one case (GRB 991023) even exceed $M_\odot c^2$. Such extreme energies in an ultrarelativistic outflow are hard to produce in models involving stellar mass progenitors. If the outflow is collimated into a narrow jet that occupies a small fraction, $f_b \ll 1$, of the total solid angle, then the strong relativistic beaming due to the very high initial Lorentz factor ($\Gamma_0 \gtrsim 100$) causes the emitted gamma rays to be similarly collimated. This reduces the true energy output in gamma rays by a factor of f_b^{-1} to $E_\gamma = f_b E_{\gamma,\rm iso}$, thus significantly reducing the energy requirements. A more direct line of evidence in favor of a narrowly collimated outflow comes from achromatic breaks seen in the afterglow light curves of many GRBs (Rhoads 1997, 1999; Sari et al. 1999).

Since the initial discovery of GRB afterglows in the X-ray (Costa et al. 1997), optical (van Paradijs et al. 1997), and radio (Frail et al. 1997), many afterglows have been detected and the quality of individual afterglow light curves has improved dramatically (e.g., Lipkin et al. 2004). Despite all the observational and theoretical progress, the structure of GRB jets remains largely an open question. This question is of great importance and interest, as it is related to issues that are fundamental for our understanding of GRBs, such as their event rate, total energy, and the requirements from the compact source that accelerates and collimates these jets.

The leading models for the jet structure are (1) the uniform jet (UJ) model (Rhoads 1997, 1999; Panaitescu & Mészáros 1999; Sari et al. 1999; Kumar & Panaitescu 2000; Moderski et al. 2000; Granot et al. 2001, 2002), where the energy per solid angle, ϵ, and the initial Lorentz factor, Γ_0, are uniform within some finite half-opening angle, θ_j, and sharply drop outside of θ_j; and (2) the universal structured jet (USJ) model (Lipunov et al. 2001; Rossi et al. 2002; Zhang & Mészáros 2002), where ϵ and Γ_0 vary smoothly with the angle θ from the jet symmetry axis. In the UJ model the different values of the jet break time, t_j, in the afterglow light curve arise mainly due to different θ_j (and to a lesser extent due to different ambient densities). In the USJ model, all GRB jets are intrinsically identical, and the different values of t_j arise mainly due to different viewing angles, $\theta_{\rm obs}$, from the jet axis.[1] The observed correlation, $t_j \propto E_{\gamma,\rm iso}^{-1}$ (Frail et al. 2001; Bloom et al. 2003), implies a roughly constant true energy, E, between different GRB jets in the UJ model, and $\epsilon \propto \theta^{-2}$ outside of some core angle, θ_c, in the USJ model (Rossi et al. 2002; Zhang & Mészáros 2002). This is assuming a constant efficiency, ϵ_γ, for producing the observed prompt gamma-ray or X-ray emission. If the efficiency ϵ_γ depends on θ in the USJ model, for example, then different power laws of ϵ with θ are possible (Guetta et al. 2005), such as a core with wings where $\epsilon \propto \theta^{-3}$, as is obtained in simulations of the collapsar model (Zhang et al. 2003, 2004b).

Other jet[2] structures have also been proposed in the literature. A jet with a Gaussian angular profile (Kumar & Granot 2003;

[1] In fact, the expression for t_j is similar to that for a uniform jet with $\epsilon \to \epsilon(\theta = \theta_{\rm obs})$ and $\theta_j \to \theta_{\rm obs}$.

[2] Throughout this work the word "jet" is used to describe any significantly nonspherical outflow.

Zhang & Mészáros 2002) may be thought of as a more realistic version of a uniform jet, where the edges are smooth rather than sharp. A Gaussian $\epsilon(\theta)$ is approximately intermediate between the UJ and USJ models, but it is closer to the UJ model than to the USJ model with $\epsilon \propto \theta^{-2}$ in the sense that for a Gaussian $\epsilon(\theta)$ the energy in the wings of the jet is much smaller than in its core, whereas for a USJ with $\epsilon \propto \theta^{-2}$ wings there is equal energy per decade in θ at the wings. If both $\epsilon(\theta)$ and $\Gamma_0(\theta)$ have a Gaussian profile (corresponding to a constant rest mass per solid angle in the outflow), then the afterglow light curves are rather similar to those for a uniform jet (Kumar & Granot 2003). If, on the other hand, $\epsilon(\theta)$ is Gaussian while[3] $\Gamma_0(\theta) = \text{const}$, then the light curves for off-axis viewing angles (i.e., outside the core of the jet) have a much higher flux at early times, compared to a Gaussian $\Gamma_0(\theta)$ or a uniform jet, due to a dominant contribution from the emitting material along the line of sight (Granot et al. 2005). Such a jet structure was considered as a quasi-universal jet model (Zhang et al. 2004a).

Another jet structure that received some attention recently is a two-component jet model (Pedersen et al. 1998; Frail et al. 2000; Berger et al. 2003; Huang et al. 2004; Peng et al. 2005; Wu et al. 2005) with a narrow uniform jet of initial Lorentz factor $\Gamma_0 \gtrsim 100$ surrounded by a wider uniform jet with $\Gamma_0 \sim 10-30$. Theoretical motivation for such a jet structure has been found both in the context of the cocoon in the collapsar model (Ramirez-Ruiz et al. 2002) and in the context of a hydromagnetically driven neutron-rich jet (Vlahakis et al. 2003). The light curves for this jet structure have been calculated analytically (Peng et al. 2005) or semianalytically (Huang et al. 2004; Wu et al. 2005), and it has been suggested that this model can account for sharp bumps (i.e., fast rebrightening episodes) in the afterglow light curves of GRB 030329 (Berger et al. 2003) and XRF 030723 (Huang et al. 2004). A different motivation for proposing this jet structure is in order to account for the energetics of GRBs and X-ray flashes and reduce the high efficiency requirements for the internal shocks (Peng et al. 2005). Here we show that effects such as the modest degree of lateral expansion that is expected in impulsive relativistic jets and the gradual hydrodynamic transition at the deceleration epoch smoothen the resulting features in the afterglow light curve, so that they cannot produce features as sharp as those mentioned above.

More "exotic" jet structures have also been considered. One example is a jet with a cross section in the shape of a "ring," sometimes referred to as a "hollow cone" (Eichler & Levinson 2003, 2004; Levinson & Eichler 2004; Lazzati & Begelman 2005), which is uniform within $\theta_c < \theta < \theta_c + \Delta\theta$ where $\Delta\theta \ll \theta_c$. Another example is a "fan"- or "sheet"-shaped jet (Thompson 2005) where a magnetocentrifugally launched wind from the proto–neutron star, formed during the supernova explosion in the massive star progenitor, becomes relativistic as the density in its immediate vicinity drops and is envisioned to form a thin sheath of relativistic outflow that is somehow able to penetrate through the progenitor star along the rotational equator, forming a relativistic outflow within $\Delta\theta \ll 1$ around $\theta = \pi/2$ (or $\theta_c = \pi/2 - \Delta\theta/2$). We stress that this has been suggested as a possible jet structure within this model, but the final jet structure is by no means clear, and other jet structures might also be possible within this model (T. A. Thompson 2005, private communication). The various jet structures are shown schematically in Figure 1.

[3] This corresponds to a Gaussian angular distribution of the rest mass per solid angle, i.e., very little mass near the outer edge of the jet, which is the opposite of what might be expected due to mixing near the walls of the funnel in the massive star progenitor.

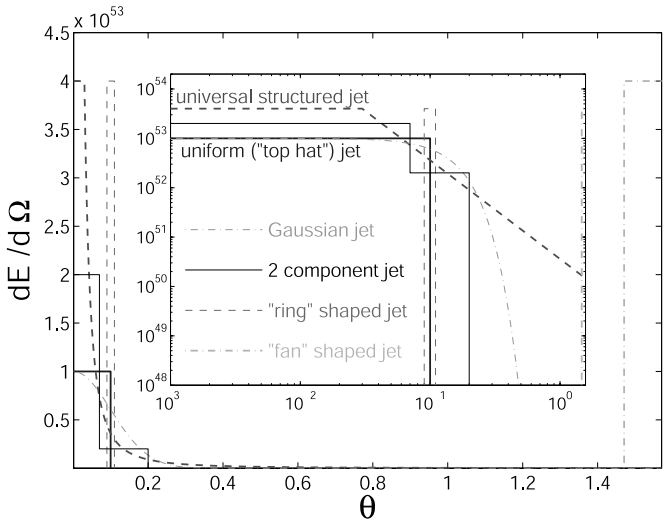

FIG. 1.—Schematic diagram of the energy per solid angle, $\epsilon = dE/d\Omega$, for the various jet structures that are discussed in this paper, shown both in a linear scale (*main figure*) and in a log-log scale (*large inset at the center*). [*See the electronic edition of the Journal for a color version of this figure.*]

The light curves for the more conventional jet structures, namely, the UJ and USJ models, as well as the Gaussian jet model, have been calculated in detail. The light curves for the less conventional jet structures, however, either have been calculated using a simple analytic or semianalytic model (for the two-component jet model) or have not been considered at all (for the ring or fan jet structures). In this paper we calculate the afterglow light curves for these models. In § 2 a simple formalism is developed for calculating the observed emission from a thin spherical relativistic shell, which includes integration over the surface of equal arrival time of photons to the observer. It is generalized to a uniform ring-shaped jet, where a finite range in θ ($\theta_c < \theta < \theta_c + \Delta\theta$) is occupied by the outflow, in § 3. The final expression for the observed flux for any viewing angle is in the form of a sum of two one-dimensional integrals, which is trivial to evaluate numerically. This formalism is used to calculate the light curves for various jet structures in § 4. In § 4.1 it is applied to a uniform jet and a two-component jet, while in §§ 4.2 and 4.3 it is used to calculate the light curves for a ring-shaped jet and a fan-shaped jet, respectively. Our conclusions are discussed in § 5.

2. CALCULATING THE LIGHT CURVE FROM A RELATIVISTIC SPHERICAL THIN SHELL

The emitting shell is assumed to be relativistic, with a Lorentz factor $\gamma = (1 - \beta^2)^{-1/2} \gg 1$, and infinitely thin, so that its location is described by its radius R as a function of the lab frame time t. The thin-shell approximation is valid in the limit where the width of the shell is $\Delta R \ll R/\gamma^2$. Typically, $\Delta R \sim R/\gamma^2$ so that the thin-shell approximation is only marginally valid, and an integration over the radial profile of the shell might introduce some changes of order unity to the resulting light curve (e.g., Granot et al. 1999; Granot & Sari 2002). In this work, however, we neglect the radial structure of the emitting shell for the sake of simplicity and in order to stress the effects of the jet angular structure.

A photon emitted at a radius R, at a lab frame time t, and at an angle θ from the line of sight reaches the observer at an observed time T, given by

$$\frac{T}{1+z} = t - \frac{R\cos\theta}{c}. \tag{1}$$

The radius is given by

$$R = c\int_0^t d\tilde{t}\,\beta(\tilde{t}) \approx ct - \int_0^R \frac{d\tilde{R}}{2\gamma^2(\tilde{R})}, \tag{2}$$

where the last expression holds in the relativistic limit ($\gamma \gg 1$). Let us assume a power-law external density profile, $\rho_{\rm ext} = AR^{-k}$.

For simplicity, it is assumed throughout the paper that the reverse shock that slows down the ejecta as it sweeps up the external medium is Newtonian or at most mildly relativistic, so that the Lorentz factor, γ, of the shocked ejecta and shocked external medium is close to η as long as the reverse shock is still crossing the ejecta shell (i.e., at $R < R_{\rm dec}$). This corresponds to the "thin-shell" case (Sari & Piran 1995; Sari 1997). For a very high initial Lorentz factor, very long GRB, or very dense external medium at $R_{\rm dec}$ as might be expected for a stellar wind of a massive star progenitor, the reverse shock might be relativistic (i.e., the "thick-shell" case). In this case the deceleration spreads over a large range in radii with an intermediate regime where $\gamma \propto R^{(k-2)/4}$, which corresponds to a solution with constant rate of energy injection at the source (Blandford & McKee 1976; Sari 1997). Once all the energy is injected, i.e., when the relativistic reverse shock finishes crossing the shell, the flow transitions into the impulsive Blandford & McKee (1976) self-similar solution where $\gamma \propto R^{(k-3)/2}$. The simple analytic dynamical model that is used in this paper, which applies to the thin-shell case, could be extended to include the thick-shell (or relativistic reverse shock) case. For brevity, this is not included in this paper. Once the deceleration takes place, however, the flow becomes self-similar (Blandford & McKee 1976) and therefore insensitive to the "thickness" of the original shell of ejecta.

The deceleration radius is given by

$$R_{\rm dec} = \left[\frac{(3-k)E_{\rm iso}}{4\pi A\eta^2 c^2}\right]^{1/(3-k)} = \begin{cases} 2.5\times10^{16} n_0^{-1/3} E_{\rm iso,52}^{1/3}\eta_{2.5}^{-2/3}\ {\rm cm} & k=0, \\ 1.8\times10^{13} A_*^{-1} E_{\rm iso,52}\eta_{2.5}^{-2}\ {\rm cm} & k=2, \end{cases} \tag{3}$$

where $\eta = 10^{2.5}\eta_{2.5}$ is the initial Lorentz factor, $E_{\rm iso} = 10^{52}E_{\rm iso,52}$ is the isotropic equivalent energy, $n = n_0\ {\rm cm}^{-3}$ is the external density for a uniform external medium ($k = 0$), and $A = 5\times10^{11}A_*$ g cm^{-1} for a stellar wind environment ($k = 2$). The corresponding observed deceleration time is

$$T_{\rm dec} = (1+z)\frac{R_{\rm dec}}{2c\eta^2} = \begin{cases} 4.2(1+z)n_0^{-1/3}E_{\rm iso,52}^{1/3}\eta_{2.5}^{-8/3}\ {\rm s} & k=0, \\ 3.0\times10^{-3}(1+z)A_*^{-1}E_{\rm iso,52}\eta_{2.5}^{-4}\ {\rm s} & k=2. \end{cases} \tag{4}$$

The Lorentz factor as a function of radius is given by (Blandford & McKee 1976)

$$\gamma(R) \approx \begin{cases} \eta & R < R_{\rm dec}, \\ \eta(R/R_{\rm dec})^{-(3-k)/2} & R > R_{\rm dec}. \end{cases} \tag{5}$$

If the bulk velocity of the emitting fluid is in the radial direction, as we assume here, then the flux density is given by[4]

$$\begin{aligned} F_\nu(T) &= \frac{(1+z)}{d_L^2(z)}\int d^4x\,\delta\left(t - \frac{T}{1+z} - \frac{R\cos\theta}{c}\right)\frac{j'_{\nu'}}{\gamma^2(1-\beta\cos\theta)^2} \\ &= \frac{(1+z)}{4\pi d_L^2(z)}\int dt\,\delta\left(t - \frac{T}{1+z} - \frac{R\cos\theta}{c}\right)\int\frac{dL'_{\nu'}}{\gamma^3(1-\beta\cos\theta)^3}, \end{aligned} \tag{6}$$

where primed quantities are measured in the local rest frame of the emitting fluid, $j'_{\nu'}$ is the spectral emissivity (emitted energy per unit volume, frequency, time, and solid angle), $L'_{\nu'}$ is in the spectral luminosity (the total emitted energy per unit time and frequency, assuming a spherical emitting shell), z and $d_L(z) = 10^{28}d_{L28}$ cm are the redshift and luminosity distance of the source, respectively, and $\nu' = (1+z)\gamma(1-\beta\cos\theta)\nu$. We have $dL'_{\nu'} = L'_{\nu'}(R)d\phi\,d\cos\theta/4\pi$, where $L'_{\nu'}(R) \propto R^a(\nu')^b$ and the values of the power-law indices a and b depend on the power-law segment of the spectrum (Sari 1998) and are calculated explicitly below.

For simplicity we ignore the self-absorption frequency and assume that the spectrum at any given time is described by three power-law segments that are divided by two break frequencies, ν_m and ν_c (Sari et al. 1998). We also consider only the emission from the shocked external medium and do not take into account the emission from the reverse shock. Now, $L'_{\nu',\max} \propto B'N_e$, where $B' \propto \gamma\rho_{\rm ext}^{1/2}$ is the magnetic field (which is assumed to hold a constant fraction, ϵ_B, of the internal energy in the shocked matter) and $N_e \propto R^{3-k}$ is the total number of emitting electrons behind the forward shock. Also, $\nu'_m \propto B'\gamma_m^2 \propto B'\gamma^2$ and $\nu'_c \propto B'\gamma_c^2 \propto \gamma^{-1}R^{3k/2-2}$, which imply

$$L'_{\nu',\max} \propto \begin{cases} R^{3-3k/2} & R < R_{\rm dec}, \\ R^{3/2-k} & R > R_{\rm dec}, \end{cases} \tag{7}$$

$$\nu'_m \propto \begin{cases} R^{-k/2} & R < R_{\rm dec}, \\ R^{-(9-2k)/2} & R > R_{\rm dec}, \end{cases} \tag{8}$$

$$\nu'_c \propto \begin{cases} R^{3k/2-2} & R < R_{\rm dec}, \\ R^{k-1/2} & R > R_{\rm dec}. \end{cases} \tag{9}$$

For fast cooling ($\nu_c < \nu_m$) we find

$$L'_{\nu'}(R < R_{\rm dec}) \propto \begin{cases} R^{11/3-2k}(\nu')^{1/3} & \nu' < \nu'_c, \\ R^{2-3k/4}(\nu')^{-1/2} & \nu'_c < \nu' < \nu'_m, \\ R^{2-k(p+2)/4}(\nu')^{-p/2} & \nu' > \nu'_m, \end{cases} \tag{10}$$

$$L'_{\nu'}(R > R_{\rm dec}) \propto \begin{cases} R^{(5-4k)/3}(\nu')^{1/3} & \nu' < \nu'_c, \\ R^{(5-2k)/4}(\nu')^{-1/2} & \nu'_c < \nu' < \nu'_m, \\ R^{[14-9p+2k(p-2)]/4}(\nu')^{-p/2} & \nu' > \nu'_m, \end{cases} \tag{11}$$

[4] More generally, $\beta\cos\theta$ should be replaced by $\hat{\boldsymbol{n}}\cdot\boldsymbol{\beta}$, where $\hat{\boldsymbol{n}}$ is the direction to the observer (in the lab frame), and if the angle θ is not measured from the line of sight, then $R\cos\theta$ should be replaced by $\hat{\boldsymbol{n}}\cdot\boldsymbol{r}$.

TABLE 1
THE RADIAL DEPENDENCE OF THE LOCAL REST-FRAME SPECTRAL LUMINOSITY

PLS	b	a ($R < R_{\rm dec}$)	a ($R > R_{\rm dec}$)
D.....	$1/3$	$3 - k/2$	$3 - 4k/3$
E.....	$1/3$	$11/3 - 2k$	$(5 - 4k)/3$
F.....	$-1/2$	$2 - 3k/4$	$(5 - 2k)/4$
G.....	$(1 - p)/2$	$3 - k(p + 5)/4$	$[15 - 9p - 2k(3 - p)]/4$
H.....	$-p/2$	$2 - k(p + 2)/4$	$[14 - 9p + 2k(p - 2)]/4$

NOTES.—The luminosity in the local rest frame of the emitting fluid behind the afterglow shock scales as a power law in frequency and in radius, $L'_{\nu'} \propto R^a(\nu')^b$, where the power-law indices a and b change between the different power-law segments (PLSs) of the spectrum. In addition, a also changes between $R < R_{\rm dec}$ and $R > R_{\rm dec}$. The first column labels the power-law segment of the spectrum following the notation of Granot & Sari (2002). The second column provides the value of spectral index b, while the third and fourth columns give the value of a for $R < R_{\rm dec}$ and $R > R_{\rm dec}$, respectively.

while for slow cooling ($\nu_c > \nu_m$) we have

$$L'_{\nu'}(R < R_{\rm dec}) \propto \begin{cases} R^{3-k/2}(\nu')^{1/3} & \nu' < \nu'_m, \\ R^{3-k(p+5)/4}(\nu')^{(1-p)/2} & \nu'_m < \nu' < \nu'_c, \\ R^{2-k(p+2)/4}(\nu')^{-p/2} & \nu' > \nu'_c, \end{cases} \tag{12}$$

$$L'_{\nu'}(R > R_{\rm dec}) \propto \begin{cases} R^{3-4k/3}(\nu')^{1/3} & \nu' < \nu'_m, \\ R^{[15-9p-2k(3-p)]/4}(\nu')^{(1-p)/2} & \nu'_m < \nu' < \nu'_c, \\ R^{[14-9p+2k(p-2)]/4}(\nu')^{-p/2} & \nu' > \nu'_c, \end{cases} \tag{13}$$

where p is the power-law index of the electron energy distribution. The values of a and b that are defined by $L'_{\nu'}(R) \propto R^a(\nu')^b$ are given in Table 1. The value of a changes at radii corresponding to hydrodynamic transitions, such as $R_{\rm dec}$, where the ejecta stops coasting and starts to decelerate significantly. If there is significant lateral spreading at R_j (the radius associated with the jet break time, T_j, in the afterglow light curve), then this would cause a change in the value of a between $R_{\rm dec} < R < R_j$ and $R_j < R < R_{\rm NR}$. A similar change in the value of a occurs at the radius of the nonrelativistic transition, $R_{\rm NR}$. In this work, however, we concentrate on the relativistic regime ($\gamma \gg 1$ and $R \ll R_{\rm NR}$).

3. CALCULATING THE LIGHT CURVES FROM A JET WITH A UNIFORM RING ANGULAR PROFILE

We now specify for a jet with an angular profile of a uniform ring, with an inner half-opening angle θ_c and an angular width $\Delta\theta$,

$$\epsilon = \frac{dE}{d\Omega} = \begin{cases} \epsilon_0 & \theta_c < \tilde{\theta} < \theta_c + \Delta\theta, \\ 0 & \text{otherwise}, \end{cases} \tag{14}$$

where $\tilde{\theta}$ is the angle from the symmetry axis of the jet, which is located at an angle $\theta_{\rm obs}$ from the line of sight. Assuming a double-sided jet, the true energy is $E = 4\pi[\cos\theta_c - \cos(\theta_c + \Delta\theta)]\epsilon_0 \approx 2\pi\Delta\theta(2\theta_c + \Delta\theta)\epsilon_0 \approx 4\pi\theta_c\Delta\theta\epsilon_0$, where the second (third) equality holds in the limit θ_c, $\Delta\theta \ll 1$ ($\Delta\theta \ll \theta_c$).

We note that this jet structure can be used to describe not only a ring-shaped jet but also a uniform jet with sharp edges, a two-component jet, or a fan-shaped jet. A uniform jet of half-opening angle θ_j corresponds to $\theta_c = 0$ and $\Delta\theta = \theta_j$. A two-component jet with a narrow (wide) jet component of half-opening angle θ_n (θ_w) corresponds to the sum of two rings, the first a uniform jet with $\theta_c = 0$ and $\Delta\theta = \theta_n$ and the second a ring with $\theta_c = \theta_n$ and $\Delta\theta = \theta_w - \theta_n$. A fan-shaped jet corresponds to the limit of a very thin ring, $\Delta\theta \ll \theta_c$, as long as $\gamma\theta_c \gg 1$, i.e., as long as the visible region of angle $\sim\gamma^{-1}$ around the line of sight is small compared to the half-opening angle of the ring. It can also be directly modeled by $\theta_c = \pi/2 - \Delta\theta/2$ with $\Delta\theta \ll 1$.

For simplicity, we neglect the lateral spreading of the jet. This is also motivated by the results of numerical studies (Granot et al. 2001; Kumar & Granot 2003) that show a very modest degree of lateral expansion as long as the jet is sufficiently relativistic.

For a given $T/(1+z)$, R is a function of θ alone, according to equation (1), and does not depend on the azimuthal angle ϕ. This also applies, within the jet itself, to all the physical quantities in the integrand in equation (6) that are a function of R: $L'_{\nu'}(R)$, $\gamma(R)$, and $\beta(R)$. Outside of the jet, however, there is no contribution to the flux. Therefore, we need to determine the fraction, $\Delta\phi/2\pi$, of a circle of angle θ from the line of sight that intersects the emitting ring and multiply the integrand in equation (6) by this factor. It is most convenient to work in spherical coordinates where the z-axis points to the observer and the jet axis is within the x-z plane (i.e., at $\phi = 0$). The intersection of a cone of half-opening angle θ around the line of sight with the inner and outer edges of the ring-shaped jet occurs at ϕ_1 and ϕ_2, respectively, which are given by[5]

$$\cos\phi_1 = \frac{\cos\theta_c - \cos\theta_{\rm obs}\cos\theta}{\sin\theta_{\rm obs}\sin\theta} \approx \frac{\theta_{\rm obs}^2 + \theta^2 - \theta_c^2}{2\theta_{\rm obs}\theta}, \tag{15}$$

$$\cos\phi_2 = \frac{\cos(\theta_c + \Delta\theta) - \cos\theta_{\rm obs}\cos\theta}{\sin\theta_{\rm obs}\sin\theta} \approx \frac{\theta_{\rm obs}^2 + \theta^2 - (\theta_c + \Delta\theta)^2}{2\theta_{\rm obs}\theta}, \tag{16}$$

where the second expression approximately holds when all relevant angles (θ_c, $\Delta\theta$, $\theta_{\rm obs}$, θ) are $\ll 1$. We find

$$\frac{\Delta\phi}{2\pi}(\theta_{\rm obs} = 0) = \begin{cases} 1 & \theta_c < \theta < \theta_c + \Delta\theta, \\ 0 & \text{otherwise}, \end{cases} \tag{17}$$

$$\frac{\Delta\phi}{2\pi}\left(0 < \theta_{\rm obs} < \frac{\Delta\theta}{2}\right) = \begin{cases} 0 & \theta < \theta_c - \theta_{\rm obs}, \\ 1 - \phi_1/\pi & \theta_c - \theta_{\rm obs} < \theta < \theta_c + \theta_{\rm obs}, \\ 1 & \theta_c + \theta_{\rm obs} < \theta < \theta_c + \Delta\theta - \theta_{\rm obs}, \\ \phi_2/\pi & \theta_c + \Delta\theta - \theta_{\rm obs} < \theta < \theta_c + \Delta\theta + \theta_{\rm obs}, \\ 0 & \theta > \theta_c + \Delta\theta + \theta_{\rm obs}, \end{cases} \tag{18}$$

$$\frac{\Delta\phi}{2\pi}\left(\frac{\Delta\theta}{2} < \theta_{\rm obs} < \theta_c\right) = \begin{cases} 0 & \theta < \theta_c - \theta_{\rm obs}, \\ 1 - \phi_1/\pi & \theta_c - \theta_{\rm obs} < \theta < \theta_c + \Delta\theta - \theta_{\rm obs}, \\ (\phi_2 - \phi_1)/\pi & \theta_c + \Delta\theta - \theta_{\rm obs} < \theta < \theta_c + \theta_{\rm obs}, \\ \phi_2/\pi & \theta_c + \theta_{\rm obs} < \theta < \theta_c + \Delta\theta + \theta_{\rm obs}, \\ 0 & \theta > \theta_c + \Delta\theta + \theta_{\rm obs}, \end{cases} \tag{19}$$

[5] Let $\hat{\boldsymbol{n}}(\theta, \phi) = \hat{\boldsymbol{z}}\cos\theta + \hat{\boldsymbol{y}}\sin\theta\sin\phi + \hat{\boldsymbol{x}}\sin\theta\cos\phi$ be a unit vector in the direction described by the angles (θ, ϕ) in polar coordinates. The inner and outer edges of the ring-shaped jet are given by $\cos\alpha = \hat{\boldsymbol{n}}(\theta_{\rm obs}, 0)\cdot\hat{\boldsymbol{n}}(\theta, \phi) = \cos\theta_{\rm obs}\cos\theta + \sin\theta_{\rm obs}\sin\theta\cos\phi$, where $\alpha = \theta_c$ and $\theta_c + \Delta\theta$ for the inner and outer edges of the jet, respectively. Now for a given value of θ this gives us the value of ϕ at which a cone of half-opening angle θ around the line of sight intersects the inner and outer edges of the jet: $\cos\phi = (\cos\alpha - \cos\theta_{\rm obs}\cos\theta)/\sin\theta_{\rm obs}\sin\theta$.

$$\frac{\Delta\phi}{2\pi}\left(\theta_c<\theta_{\rm obs}<\theta_c+\frac{\Delta\theta}{2}\right)=\begin{cases}1 & \theta<\theta_{\rm obs}-\theta_c,\\ 1-\phi_1/\pi & \theta_{\rm obs}-\theta_c<\theta<\theta_c+\Delta\theta-\theta_{\rm obs},\\ (\phi_2-\phi_1)/\pi & \theta_c+\Delta\theta-\theta_{\rm obs}<\theta<\theta_c+\theta_{\rm obs},\\ \phi_2/\pi & \theta_c+\theta_{\rm obs}<\theta<\theta_c+\Delta\theta+\theta_{\rm obs},\\ 0 & \theta>\theta_c+\Delta\theta+\theta_{\rm obs},\end{cases}\quad(20)$$

$$\frac{\Delta\phi}{2\pi}\left(\theta_c+\frac{\Delta\theta}{2}<\theta_{\rm obs}<\theta_c+\Delta\theta\right)=\begin{cases}1 & \theta<\theta_c+\Delta\theta-\theta_{\rm obs},\\ \phi_2/\pi & \theta_c+\Delta\theta-\theta_{\rm obs}<\theta<\theta_{\rm obs}-\theta_c,\\ (\phi_2-\phi_1)/\pi & \theta_{\rm obs}-\theta_{\rm c}<\theta<\theta_{\rm c}+\theta_{\rm obs},\\ \phi_2/\pi & \theta_c+\theta_{\rm obs}<\theta<\theta_c+\Delta\theta+\theta_{\rm obs},\\ 0 & \theta>\theta_c+\Delta\theta+\theta_{\rm obs},\end{cases}\quad(21)$$

$$\frac{\Delta\phi}{2\pi}(\theta_{\rm obs}>\theta_c+\Delta\theta)=\begin{cases}0 & \theta<\theta_{\rm obs}-\theta_c-\Delta\theta,\\ \phi_2/\pi & \theta_{\rm obs}-\theta_c-\Delta\theta<\theta<\theta_{\rm obs}-\theta_c,\\ (\phi_2-\phi_1)/\pi & \theta_{\rm obs}-\theta_c<\theta<\theta_c+\theta_{\rm obs},\\ \phi_2/\pi & \theta_c+\theta_{\rm obs}<\theta<\theta_c+\Delta\theta+\theta_{\rm obs},\\ 0 & \theta>\theta_c+\Delta\theta+\theta_{\rm obs}.\end{cases}\quad(22)$$

It is more convenient to integrate over R, instead of over θ. In the relativistic limit,

$$\frac{T}{1+z}\approx\begin{cases}\dfrac{R}{2\eta^2c}\left(1+\eta^2\theta^2\right) & R<R_{\rm dec},\\ \dfrac{R}{2\gamma^2c}\left[\dfrac{1}{(4-k)}+\gamma^2\theta^2\right]+\left(\dfrac{3-k}{4-k}\right)\dfrac{R_{\rm dec}}{2\eta^2c}= & \\ \quad\dfrac{R_L}{2(4-k)\gamma_L^2c}\left[(4-k)\gamma_L^2\theta^2x\right. & \\ \quad\left.+x^{4-k}+(3-k)x_{\rm dec}^{4-k}\right] & R>R_{\rm dec},\end{cases}\quad(23)$$

where $\gamma_L=\gamma(R_L)$ and $R_L(T)$ are the Lorentz factor and radius from which a photon emitted along the line of sight (at $\theta=0$) reaches the observer at an observed time T, while $x\equiv R/R_L$ and $x_{\rm dec}\equiv R_{\rm dec}/R_L$. We have

$$R_L(T)=\frac{2cT}{1+z}\begin{cases}\eta^2 & T<T_{\rm dec},\\ \dfrac{(4-k)\gamma_L^2}{1+(3-k)x_{\rm dec}^{4-k}} & T>T_{\rm dec},\end{cases}\quad(24)$$

$$x_{\rm dec}=\left[(4-k)T/T_{\rm dec}-(3-k)\right]^{-1/(4-k)},\quad(25)$$

and thus obtain

$$\theta^2=\begin{cases}\dfrac{x^1-1}{\eta^2} & R<R_{\rm dec},\\ \dfrac{1}{(4-k)\gamma_L^2}(x^{-1}-x^{3-k}) & R>R_{\rm dec}.\end{cases}\quad(26)$$

Therefore, $d\cos\theta\approx d(\theta^2)/2=dx[d(\theta^2)/dx]/2$, where

$$\frac{d\cos\theta}{dx}\approx\frac{1}{2}\frac{d(\theta^2)}{dx}=\begin{cases}-(cT/R_L)x^{-2} & x<x_{\rm dec},\\ -\dfrac{x^{-2}+(3-k)x^{2-k}}{2(4-k)\gamma_L^2} & x>x_{\rm dec}.\end{cases}\quad(27)$$

Finally, we can express the integral for the flux density as[6]

$$\begin{aligned}F_\nu(T)&=\frac{1}{4\pi D^2}\int\frac{dL'_{\nu'}}{\gamma^3(1-\beta\cos\theta)^3}\\&=\frac{1}{8\pi D^2}\int_0^{R_L(T)}dR\left|\frac{d\cos\theta}{dR}\right|\delta^3(R)L'_{\nu'}(R)\frac{\Delta\phi[\theta(R)]}{2\pi}\\&=\frac{1}{8\pi D^2}\int_0^1dx\left|\frac{d\cos\theta}{dx}\right|\delta^3L'_{\nu'}\left(\frac{\Delta\phi}{2\pi}\right),\end{aligned}\quad(28)$$

where $\delta\equiv\nu/\nu'=1/\gamma(1-\beta\cos\theta)\approx2\gamma/(1+\gamma^2\theta^2)$ is the Doppler factor, which is given by

$$\delta=\begin{cases}2\eta x & x<x_{\rm dec},\\ \dfrac{2(4-k)\gamma_Lx^{(k-3)/2}}{4-k+x^{k-4}-1} & x>x_{\rm dec}.\end{cases}\quad(29)$$

For $T<T_{\rm dec}$ we have $R_L=2\eta^2cT<2\eta^2cT_{\rm dec}=R_{\rm dec}$ and

$$L'_{\nu/\delta}(R)=L'_{\nu/2\eta}(R_L)x^a[\delta/2\eta]^{-b}=L'_{\nu/2\eta}(R_L)x^{a-b},$$

and therefore

$$\begin{aligned}F_\nu(T)&=\frac{2\eta L'_{\nu/2\eta}[R_L(T)]}{4\pi D^2}\int_0^1dx\,x^{1+a-b}\frac{\Delta\phi(x)}{2\pi}\\&=\frac{2\eta L'_{\nu/2\eta}(R_{\rm dec})}{4\pi D^2}\left(\frac{T}{T_{\rm dec}}\right)^a\int_0^1dx\,x^{1+a-b}\frac{\Delta\phi(x)}{2\pi}.\end{aligned}\quad(30)$$

As long as the outer edge of the ring is not seen, $\Delta\phi/2\pi=1$, and we have a result similar to the spherical case, where $F_\nu(T)\propto T^a$.

For $T>T_{\rm dec}$ we have $R_L(T)>R_{\rm dec}$, and the integral in equation (6) naturally divides into two terms, corresponding to $R<R_{\rm dec}$ and $R_{\rm dec}<R<R_L$, respectively. Therefore,

$$\begin{aligned}F_\nu(T)=\frac{2\eta L'_{\nu/2\eta}(R_{\rm dec})}{4\pi D^2}&\left\{\left(\frac{T}{T_{\rm dec}}\right)^{b-2}\right.\\&\times\int_0^1dy\,y^{1+a-b}\frac{\Delta\phi(y)}{2\pi}+x_{\rm dec}^{-a+(1-b)(3-k)/2}\\&\left.\times\int_{x_{\rm dec}}^1dx\,x^{a-2+(3-b)(5-k)/2}\left[\frac{1+(3-k)x^{4-k}}{(4-k)}\right]^{b-2}\frac{\Delta\phi(x)}{2\pi}\right\},\end{aligned}\quad(31)$$

where $y=R/R_{\rm dec}$, and it should be noted that the values of a are generally different in the two integrals. The values of b may also change in the middle of each of the two integrals, in which case this would require to divide the range of integration accordingly and use the appropriate value of b in each subrange. From equation (31) it can be seen that the second term dominates

[6] For simplicity, from this point on we drop all the cosmological corrections and simply denote the distance to the source by D (they can easily be put back in at the final result, according to eq. [6]).

at $T \gg T_{\rm dec}$, which in the spherical case (where $\Delta\phi/2\pi = 1$) implies

$$F_\nu \propto x_{\rm dec}^{-a+(1-b)(3-k)/2} \propto T^{-[-a+(1-b)(3-k)/2]/(4-k)},$$

since $x_{\rm dec} \propto 1/R_L(T) \propto T^{-1/(4-k)}$.

Please note that $2\eta L'_{\nu/2\eta}(R_{\rm dec}) = L_\nu(R_{\rm dec},\ \theta = 0)$, which means that the coefficient in front of the integrals in equations (30) and (31) is approximately[7] $F_\nu(T_{\rm dec})$, for a viewing angle within the jet, which can be calculated from the corresponding values of the peak flux and break frequencies,

$$F_{\nu,\max}(T_{\rm dec}) = \begin{cases} 7.8(1+z)\epsilon_{B,-2}^{1/2} n_0^{1/2} E_{\rm iso,52} d_{L28}^{-2}\ {\rm mJy} & k = 0, \\ 2.4\times10^5(1+z)\epsilon_{B,-2}^{1/2} A_*^{3/2} \eta_{2.5}^2 d_{L28}^{-2}\ {\rm mJy} & k = 2, \end{cases} \quad (32)$$

$$\nu_m(T_{\rm dec}) = \begin{cases} 4.1\times10^{18} g^2(1+z)^{-1} \\ \quad \times \epsilon_{B,-2}^{1/2}\epsilon_{e,-1}^2 n_0^{1/2}\eta_{2.5}^4\ {\rm Hz} & k = 0, \\ 1.3\times10^{23} g^2(1+z)^{-1}\epsilon_{B,-2}^{1/2}\epsilon_{e,-1}^2 \\ \quad \times A_*^{3/2} E_{\rm iso,52}^{-1}\eta_{2.5}^6 d_{L28}^{-2}\ {\rm Hz} & k = 2, \end{cases} \quad (33)$$

$$\nu_c(T_{\rm dec}) = \begin{cases} 1.6\times10^{17}(1+z)^{-1}(1+Y)^{-2} \\ \quad \times \epsilon_{B,-2}^{-3/2} n_0^{-5/6} E_{\rm iso,52}^{-2/3}\eta_{2.5}^{4/3}\ {\rm Hz} & k = 0, \\ 1.1\times10^{10}(1+z)^{-1}(1+Y)^{-2} \\ \quad \times \epsilon_{B,-2}^{-3/2} A_*^{-5/2} E_{\rm iso,52}\eta_{2.5}^{-2}\ {\rm Hz} & k = 2, \end{cases} \quad (34)$$

where $g = 3(p-2)/(p-1)$, Y is the Compton y-parameter, and $\epsilon_e = 0.1\epsilon_{e,-1}$ ($\epsilon_B = 0.01\epsilon_{B,-1}$) is the fraction of the internal energy behind the shock in relativistic electrons (the magnetic field).

4. RESULTS

4.1. *A Two-Component Jet*

The two-component jet model has been suggested as an explanation for sharp rebrightening features in the afterglow light curves of XRF 030723 (Huang et al. 2004) and GRB 030329 (Berger et al. 2003). For XRF 030723, Huang et al. (2004) suggested that our line of sight is slightly outside the wide jet, so that the beaming cone of the radiation from the wide jet expands enough to include the line of sight early on, while that of the narrow jet does so at a significantly later time, causing a bump in the light curve[8] that might account for the sharp bump seen in the optical afterglow light curve of XRF 030723 at $T \sim 15$ days.

In Figure 2 we show the light curve calculated using the model from § 3 with the parameters of the best-fit model from Huang et al. (2004), which clearly shows that the resulting bump in the light curve is very smooth. The main cause for the smoother bump in the light curve compared to the results of Huang et al. (2004) is that they assumed a relativistic lateral expansion of the jet in its own rest frame, while in the model that is used here there is no lateral expansion. The lateral expansion causes the beaming cone of the emitting material at the edge of the jet to approach a line of sight initially outside of the jet faster, since (1) the jet Lorentz factor decreases faster with radius and with observed time, and (2) the edge of the jet gets closer to the line of sight as the jet expands laterally. This causes a much sharper bump in the light curve for relativistic lateral expansion in the local frame.

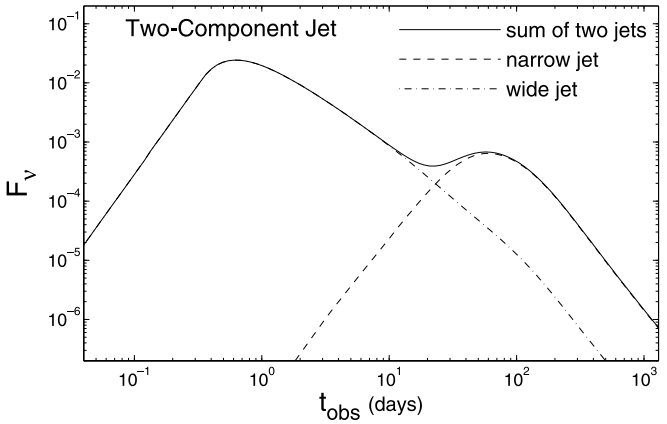

FIG. 2.—Optical light curve for a two-component jet model. The physical parameters of the jet were taken from the best-fit model of Huang et al. (2004) to the optical light curve of XRF 030723: $\theta_n = 0.09$, $\theta_w = 0.3$, $\theta_{\rm obs} = 0.37$, $E_{n,\rm iso} = 3\times10^{53}$ ergs, $E_{w,\rm iso} = 10^{52}$ ergs, $k = 0$, $n_0 = 1$, and $p = 3.2$. The exact values of ϵ_e and ϵ_B affect the flux normalization but not the shape of the light curve, as long as a break frequency does not pass through the observed frequency band, as is assumed here since we use a constant $b = (1-p)/2$.

Hydrodynamical simulations of the jet dynamics show only very modest lateral expansion as long as the jet is relativistic (Granot et al. 2001), and the resulting peak in the light curve as the beaming cone of the jet material reaches a line of sight initially outside of the jet is very broad and smooth (see Fig. 2 of Granot et al. 2002). Thus, under realistic conditions this scenario cannot produce the very sharp rise in the flux at the onset of the observed rebrightening in the optical afterglow of XRF 030723 (Fynbo et al. 2004). An alternative explanation for this bump in the light curve is a contribution from an underlying supernova component, which naturally produces the red colors that were observed during the bump (Fynbo et al. 2004) and could also potentially produce a sharp enough rise to the bump (Tominaga et al. 2004).

For GRB 030329, Berger et al. (2003) suggested that the sharp bump in the optical afterglow light at $T \sim 1.5$ days (Lipkin et al. 2004) is due to a two-component jet model where our line of sight is within the narrow jet and the bump in the light curve occurs at the deceleration time of the wide jet, $T_{\rm dec,w}$. In Figure 3 we show the optical light curve for our model from § 3 using parameters similar to those used by Berger et al. (2003). Despite the fact that our model assumes an abrupt hydrodynamic transition at the deceleration time, between the early coasting phase and the subsequent self-similar deceleration phase, the rise to the bump in the light curve is not sharp enough to match the observations. If a more gradual hydrodynamic transition at $T_{\rm dec,w}$ is assumed, as is shown in Figure 4 using model 1 of Granot & Kumar (2003), this produces a much smoother bump in the light curve, which is in a much stronger contrast with the observed sharp bump. A much more likely explanation for the bump in the optical light curve of GRB 030329, which can also account for the subsequent bumps in the following days and for the duration of these bumps, is refreshed shocks (Granot et al. 2003). Such refreshed shocks may naturally arise in a neutron-rich hydromagnetic outflow (Vlahakis et al. 2003; Peng et al. 2005), which also naturally produces a two-component jet

[7] This is only approximate since there are significant contributions to the observed flux from $\theta \lesssim \gamma^{-1}$ from which the Doppler factor is somewhat lower than its value exactly along the line of sight at $\theta = 0$.

[8] We note that in this scenario the true energy of the narrow jet must be larger than that of the wide jet in order to produce a bump in the afterglow light curve (Peng et al. 2005).

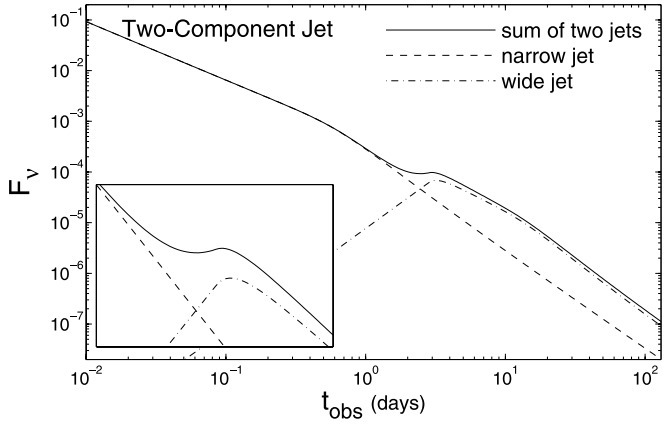

FIG. 3.—Optical light curve for a two-component jet model were the physical parameters of the jet were taken to be similar to those used by Berger et al. (2003) in order to account for the multifrequency afterglow light curves of GRB 030329, namely, $\theta_n = 0.09$, $\theta_w = 0.3$, $\theta_{\rm obs} = 0$, $E_{n,\rm iso} = 1.2\times10^{52}$ ergs, $E_{w,\rm iso} = 5.6\times10^{51}$ ergs, $\eta_w = 6.5$, $k = 0$, $n_0 = 1.8$, $p = 2.2$, and $b = -p/2$. The inset shows a close-up of the bump in the light curve that occurs near the deceleration time of the wide jet, as its emission starts to dominate the observed flux.

structure. Thus, we conclude that both a jet viewed off-axis becoming visible and the deceleration of a jet viewed on-axis produce smooth bumps in the afterglow light curves and cannot account for very sharp features.

4.2. *A Ring-shaped Jet*

Figure 5 shows the light curves for a jet with an angular profile of a thin uniform ring, using the model from § 3. The jet occupies $\theta_c < \theta < \theta_c + \Delta\theta$, where in the example shown in Figure 5, $\theta_c = 0.1$, $\Delta\theta = 0.01$, and $\eta = 10^3$. For viewing angles within the jet itself, $\theta_c \le \theta_{\rm obs} \le \theta_c + \Delta\theta$, the light curves have a rather small dependence on the exact value of the viewing angle, $\theta_{\rm obs}$. In fact, the light curves for lines of sight at the inner edge ($\theta_{\rm obs} = 0.1$) and outer edge ($\theta_{\rm obs} = 0.11$) of the ring are practically one on top of the other. The deceleration time occurs early on.

The "jet break" in the light curve breaks up into two separate and smaller steepening epochs. The first steepening of the light curve occurs at T_{j1}, when both edges of the ring become visible, i.e., when $\gamma\Delta\theta \sim 1$ for a line of sight near the inner or outer edge of the ring, and when $\gamma\Delta\theta \sim 2$ for a line of sight midway

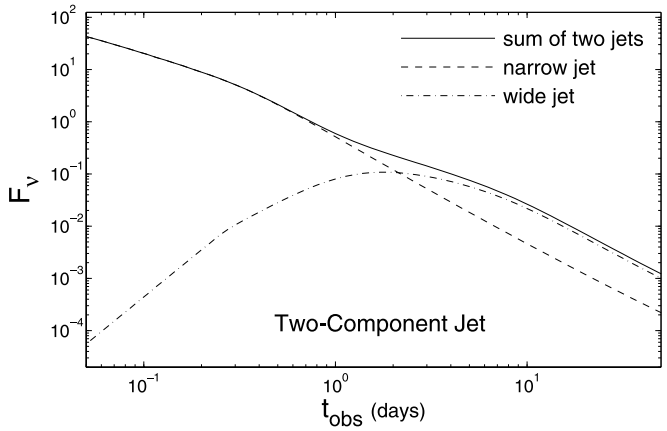

FIG. 4.—Similar to Fig. 3, but using a different numerical code (model 1 of Granot & Kumar 2003) that features a more gradual dynamical transition at the deceleration time, resulting in a much smoother bump in the light curve near $T_{\rm dec,w}$.

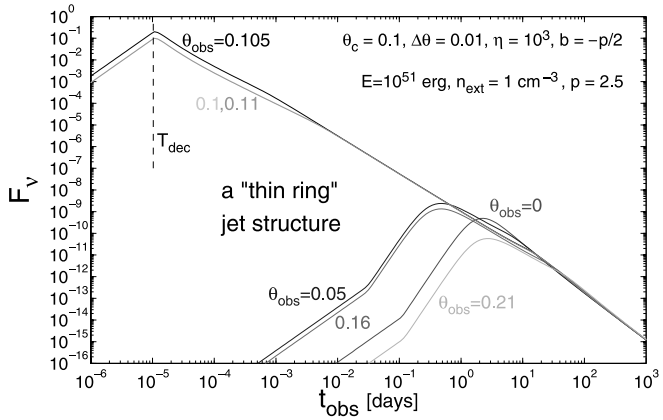

FIG. 5.—Light curves for a jet with a structure of a thin uniform ring, using the model from § 3. The vertical dashed line indicates the deceleration time, $T_{\rm dec}$. [*See the electronic edition of the Journal for a color version of this figure.*]

across the width of the ring ($\theta_{\rm obs} = \theta_c + \Delta\theta/2$). After T_{j1} the light curves from all of the viewing angles within the jet itself ($\theta_c \le \theta_{\rm obs} \le \theta_c + \Delta\theta$) become practically indistinguishable, while before T_{j1} there are small differences, up to a factor of 2. The second steepening of the light curve occurs at T_{j2}, when all of the jet becomes visible, i.e., when $\gamma\theta_c \sim \frac{1}{2}$. The light curves from $\theta_{\rm obs} = 0$ and $\theta_{\rm obs} = 2\theta_c + \Delta\theta \approx 2\theta_c$ join those for $\theta_c \le \theta_{\rm obs} \le \theta_c + \Delta\theta$ at a slightly earlier time when $\gamma\theta_c \sim 1$, while the light curves from $\theta_{\rm obs} = \theta_c/2$ or $\theta_{\rm obs} = 1.5\theta_c + \Delta\theta$ join in earlier on, when $\gamma\theta_c \sim 2$. The fact that the jet break is divided into two distinct steepening epochs in the light curve, with half of the total steepening at each epoch, implies that this model cannot reproduce the large steepening at a single jet break time in the light curve as is observed in GRB afterglows. Therefore, this jet structure does not work well for most of the best monitored GRB afterglows.

Above we have assumed no lateral spreading of the jet. As is shown in § 4.3, relativistic lateral expansion in the local rest frame would cause a somewhat smaller steepening, $\Delta\alpha$, of the afterglow light curve across the jet break for a fan-shaped jet. This applies also to the first jet break in a thin-ring jet, for $\theta_c \le \theta_{\rm obs} \le \theta_c + \Delta\theta$, since in the limit $\Delta\theta \ll \theta_c$ the visible part of the jet near the first jet break is within an angle of $\gamma^{-1} \lesssim \Delta\theta \ll \theta_c$ around the line of sight, and this portion of the jet is locally well approximated by a segment of a fan-shaped jet. The total steepening in the afterglow light curve across both jet breaks, $\Delta\alpha_{\rm tot} = \Delta\alpha_1 + \Delta\alpha_2$, is the same as for a uniform jet and is somewhat larger for relativistic lateral expansion in the local rest frame compared to no lateral expansion (Rhoads 1999; Sari et al. 1999). Therefore, the steepening (in terms of $\Delta\alpha$) across the second jet break for relativistic lateral expansion is somewhat more than half [or more precisely, a fraction $(4-k)/(7-2k)$] of that for a conical uniform jet. This suggests that it might be marginally steep enough to reproduce the observed values of $\Delta\alpha$ in GRB afterglows. However, in this case the second jet break is expected to be gradual and extend over a wide range in times, making it hard to reconcile with the sharp observed jet breaks. Furthermore, numerical simulations show relatively little lateral expansion as long as the jet is relativistic (Granot et al. 2001).

There is, however, a theoretical motivation for a "thick-ring" jet structure (Eichler & Levinson 2003, 2004; Levinson & Eichler 2004), where $\theta_c/\Delta\theta \sim 2$–3. In Figure 6 we show the light curves for a line of sight within the jet itself ($\theta_{\rm obs} = \theta_c + \Delta\theta/2$) for different values of the ratio $\theta_c/\Delta\theta$ that correspond to

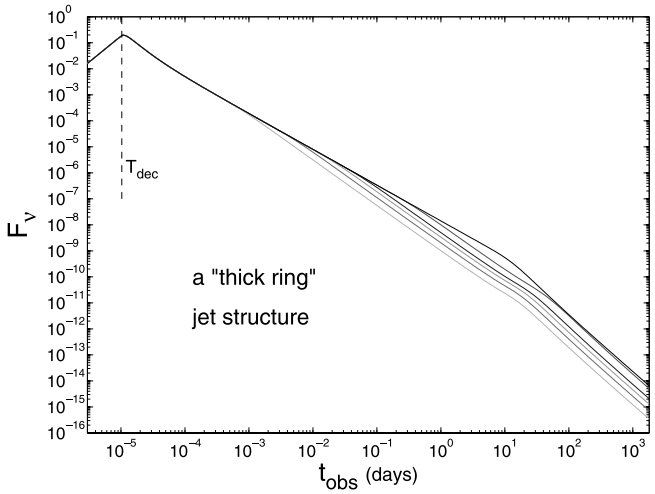

FIG. 6.—Light curves for a jet with an angular structure of a ring for various fractional widths, viewed from within the jet. The upper line is for a uniform jet viewed from along its symmetry axis ($\theta_c = \theta_{obs} = 0$, $\Delta\theta = 0.2$) and is included for comparison, while the other lines are for a ring-shaped jet with $\theta_c = 0.1$ and $\theta_c/\Delta\theta = 1$, 2, 3, 5, and 10, from top to bottom, viewed from $\theta_{obs} = \theta_c + \Delta\theta/2$. The light curves are calculated using the model from § 3 and for a constant energy per solid angle within the jet (corresponding to the same value as in Fig. 5). We also use $k = 0$, $n_0 = 1$, $b = -p/2$, and $p = 2.5$. [*See the electronic edition of the Journal for a color version of this figure.*]

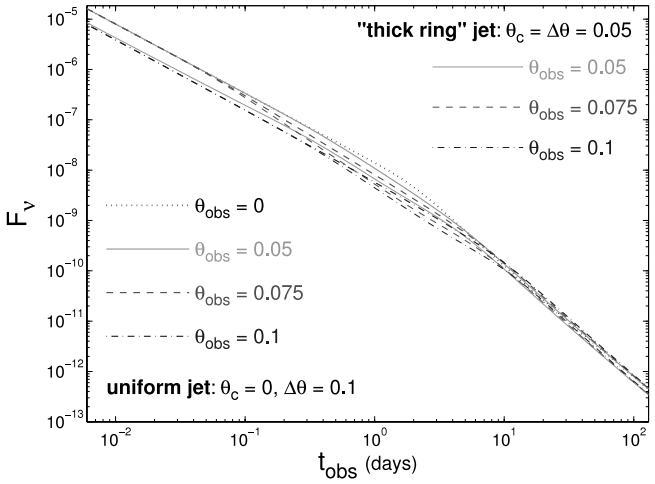

FIG. 7.—Light curves for a jet with an angular structure of a thick ring compared to those for a uniform conical jet, for different viewing angles. The light curves are calculated using the model from § 3 with $k = 0$, $n_0 = 1$, $b = -p/2$, and $p = 2.5$. The same energy per solid angle is used for the two jet structures. [*See the electronic edition of the Journal for a color version of this figure.*]

different fractional widths of the ring. We keep $\theta_c = 0.1$ and the energy per solid angle within the jet constant, while varying $\theta_c/\Delta\theta$. It can be seen that, as expected, T_{j1} is smaller for larger values of $\theta_c/\Delta\theta$ that correspond to a narrower ring, while T_{j2} remains roughly constant. We note that even for $\theta_c/\Delta\theta$ as low as 1, the two steepening epochs in the light curve, $T_{j1} < T_{j2}$, are still quite distinct and separated by $\sim$1–2 orders of magnitude in time. For comparison, we also show the light curve for a uniform jet viewed on-axis ($\theta_c = \theta_{obs} = 0$, $\Delta\theta = 0.2$), which produces a single sharp jet break in the afterglow light curve, similar to those observed in GRB afterglows.

In Figure 7 we show the light curves for a thick-ring jet ($\theta_c = \Delta\theta = 0.05$) together with those for a uniform conical jet ($\theta_c = 0$, $\Delta\theta = 0.1$) with the same outer angle and the same energy per solid angle, so that the thick-ring jet is obtained from the uniform conical jet by taking out its inner half (in terms of θ). It can be seen that the light curves for a uniform jet show a sharper jet break for viewing angle near the jet symmetry axis and somewhat smoother jet breaks for viewing angles closer to the outer edge of the jet. This result is similar to that from numerical simulations (Granot et al. 2001). By comparing the light curves for the two jet structures viewed from the same viewing angle, we can see that those for the thick-ring jet produce a somewhat lower flux as they are missing the contribution from the central part of the jet. The thick-ring jet also produces a somewhat less pronounced jet break compared to a uniform jet. However, for $\Delta\theta \gtrsim \theta_c$ the differences in the light curves compared to those for a uniform conical jet might not be large enough to easily distinguish between these two jet structures using the observed afterglow light curves. Furthermore, for $\Delta\theta \sim \theta_c$, if there is relativistic lateral expansion of the jet in its own rest frame, this might help bring T_{j1} and T_{j2} closer together, making the light curves closer to the observations. For $\Delta\theta < \theta_c$, however, the effects of lateral spreading should be rather small. We therefore conclude that a ring-shaped jet requires a very thick ring, with $\Delta\theta \gtrsim \theta_c$, in order to reproduce the observed afterglow light curves, while a jet in the shape of a thinner ring does not produce afterglow light curves with a sharp enough jet break to match afterglow observations.

4.3. *A Fan-shaped Jet*

An interesting jet structure that resembles a fan can arise due to a magnetocentrifugally launched wind that is driven by the newly formed proto–neutron star during the supernova explosion (Thompson 2005). If this wind is concentrated within a narrow angle θ_0 around the rotational equator and somehow makes it out of the star while still highly relativistic, this could create a GRB outflow within $|\tilde{\theta}| < \theta_0$, where $\tilde{\theta} = \theta - \pi/2$ is the angle from the rotational equator (i.e., the latitude). The fraction of the total solid angle that is occupied by such a jet is $f_b = \sin\tilde{\theta}_j \approx \tilde{\theta}_j$. This corresponds to a ring-shaped jet with the parameters $\theta_c = \pi/2 - \Delta\theta/2$ and $\Delta\theta = 2\theta_0$, using the notations from § 3.

If there is no lateral expansion, then the steepening during the jet break is by a factor of $\sim\gamma\theta_0 \propto T^{-(3-k)/2(4-k)}$ corresponding to $\Delta\alpha = (3-k)/2(4-k)$, which is $\frac{3}{8}$ for $k = 0$ and $\frac{1}{4}$ for $k = 2$. This is much shallower than observed in the jet breaks of GRB afterglows and exactly half as steep (in terms of $\Delta\alpha$) as the jet break for a conical uniform jet. This is demonstrated in Figure 8, which shows light curves for this jet structure that were calculated using the model from § 3. As for the ring-shaped jet, the light curves for viewing angles within the jet are similar to each other, differing by up to a factor of 2 before the jet break time and practically identical after the jet break time. In contrast to the ring-shaped jet, there is only one jet break time in the light curve, with at most half the steepening compared to a uniform conical jet. This may be understood as in the limit $\theta_c \sim \pi/2$, T_{j1} becomes similar to the time of the nonrelativistic transition and therefore does not produce a distinct break in the light curve, so that only one epoch of steepening in the light curve remains, at T_{j1}, when the edges of the fan-shaped jet become visible (i.e., when $\gamma\Delta\theta \sim 1$ for a line of sight at the edge of the jet and when $\gamma\Delta\theta \sim 2$ for a line of sight at the center of the jet). The light curves for lines of sight outside of the jet join those for lines of sight inside the jet when the beaming cone of the radiation from the jet (which extends out to an angle of $\sim 1/\gamma$ from the edges of the jet) reaches the line of sight.

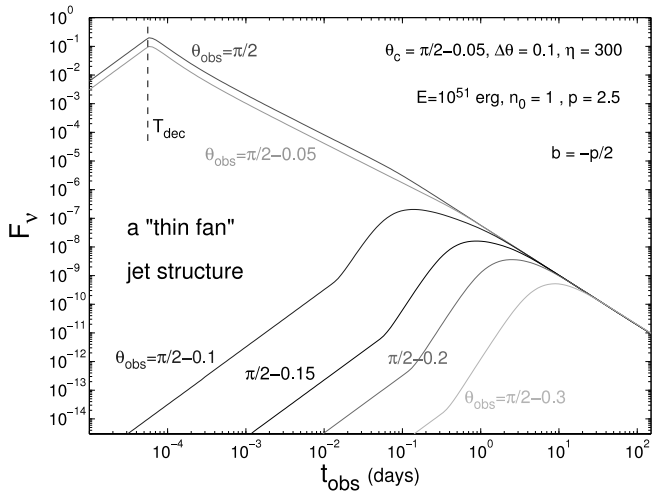

FIG. 8.—Light curves for a jet with an angular structure of a thin fan, with an opening angle of $\Delta\theta = 0.1$ centered on $\theta = \pi/2$ (i.e., $\theta_c = \pi/2 - \Delta\theta/2 = \pi/2 - 0.05$). The light curves are calculated using the model from § 3. [*See the electronic edition of the Journal for a color version of this figure.*]

For a relativistic expansion in the local rest frame we have $\tilde{\theta}_j \approx \max(\tilde{\theta}_0,\ \gamma^{-1})$ so that at $T > T_j$, $\tilde{\theta}_j \approx \gamma^{-1}$ and

$$E \approx \frac{4\pi}{(3-k)} Ac^2 R^{3-k} \gamma^2 \tilde{\theta} \approx \frac{4\pi}{(3-k)} Ac^2 R^{3-k} \gamma, \qquad (35)$$

implying

$$\gamma \propto R^{k-3} \propto T^{-(3-k)/(7-2k)}. \qquad (36)$$

This behavior is intermediate between the spherical case, $\gamma \propto T^{-(3-k)/2(4-k)}$, and the case of a narrow conical jet that expands sideways relativistically in its own rest frame, $\gamma \propto T^{-1/2}$. The temporal decay index at $T > T_j$ is also intermediate: $F_\nu \propto T^{(12-5k-24p+7kp)/4(7-2k)}$ for $\nu_m < \nu < \nu_c$ and $F_\nu \propto T^{(8-2k-24p+7kp)/4(7-2k)}$ for $\nu > \max(\nu_c,\ \nu_m)$. In both cases $\Delta\alpha$ is reduced by a factor of $(7-2k)/(3-k)$ compared to a uniform conical jet, i.e., the jet break is less than half as steep. This result is also valid for the first jet break (at T_{j1}) for a jet in the shape of a narrow ring, which was discussed in § 4.2.

Finally, we have so far assumed that the fan-shaped jet occupies all of the range of azimuthal angle φ. If it occupies a smaller range, $\Delta\varphi < 2\pi$, then as long as $\Delta\varphi \gtrsim 1$, the second jet break will overlap with the nonrelativistic transition and would not produce a distinct steepening of the light curve. For $\Delta\theta \ll \Delta\varphi \ll 1$, however, there will be two distinct jet breaks in the light curve, the first the same as described above and a second jet break when the edges of the jet in the φ-direction become visible (when $\gamma\Delta\varphi \sim 1$ for a line of sight at the edge of the jet in the φ-direction, and at $\gamma\Delta\varphi \sim 2$ for a line of sight at the center of the jet in the φ-direction).

5. CONCLUSIONS

In §§ 2 and 3 we have developed a semianalytic formalism for calculating the afterglow light curves for a jet with an angular profile of a uniform ring. The final expression for the observed flux is the sum of two one-dimensional integrals that are trivial to evaluate numerically. Despite its simplicity, this model includes integration over the surface of equal arrival time of photons to the observer, thus producing realistic results when this is indeed the dominant effect in smoothing out sharp features in the afterglow light curve.

The price of the simple expressions for the observed flux is simple assumptions on the jet dynamics, namely, no lateral expansion and an abrupt transition at the deceleration time, $T_{\rm dec}$. This results in a relatively sharp peak in the light curve at $T_{\rm dec}$, while a more realistic model for the dynamics with a smoother dynamical transition at $T_{\rm dec}$ would produce a smoother peak in the light curve (compare Figs. 3 and 4). Nevertheless, when used with care, this simple formalism may serve as a powerful tool. It may also be generalized so that it could be applicable to other jet structures, which were not considered in this work, or to include a calculation of the polarization assuming some local configuration of the magnetic field (e.g., a field tangled within the plane of the shock that is identified with the thin emitting shell).

In § 4.1 we have shown that the two-component jet model cannot produce very sharp features in the afterglow light curve, due to the deceleration of the wide (or narrow) jet, or when the narrow (or wide) jet becomes visible at lines of site outside of the jet aperture, as the beaming cone of the emitted radiation reaches the line of sight. Therefore, such explanations for the bumps in the optical light curves of GRB 030329 (Berger et al. 2003) and XRF 030723 (Huang et al. 2004), which both had a sharp rise to the bump, do not work well (see Figs. 2, 3, and 4).

The afterglow light curves for a jet with a ringlike or hollow cone angular profile were calculated in § 4.2. We find that the jet break in the light curve divides into two distinct steepening episodes, T_{j1} and T_{j2}, with roughly (or in our simple model, exactly) half of the total steepening occurring at each of these two times. The two times remain distinct even for a moderately thick ring and might merge into a single jet break in the light curve only for a very thick ring, with $\Delta\theta \gtrsim \theta_c$.

The light curves for a fan-shaped jet were calculated in § 4.3 and show a single jet break in the light curve with a very moderate steepening across the break, which is at most half of that for a "standard" conical uniform jet. The jet break is even slightly shallower when lateral expansion is taken into account, in which case it is less than half of the steepening for a conical uniform jet. Such a shallow jet break cannot account for the large steepening of the light curves that are observed in GRB afterglows.

I thank Y. F. Huang, T. A. Thompson, A. Königl, D. Eichler, and E. Ramirez-Ruiz for useful comments and the referee for many useful suggestions. This research was supported by the US Department of Energy under contract DE-AC03-76SF00515.

REFERENCES

Berger, E., et al. 2003, Nature, 426, 154
Blandford, R. D., & McKee, C. 1976, Phys. Fluids, 19, 1130
Bloom, J. S., Frail, D. A., & Kulkarni, S. R. 2003, ApJ, 594, 674
Costa, E., et al. 1997, Nature, 387, 783
Eichler, D., & Levinson, A. 2003, ApJ, 596, L147
———. 2004, ApJ, 614, L13
Frail, D. A., et al. 1997, Nature, 389, 261
———. 2000, ApJ, 538, L129
Frail, D. A., et al. 2001, ApJ, 562, L55
Fynbo, J. P. U., et al. 2004, ApJ, 609, 962
Granot, J., & Kumar, P. 2003, ApJ, 591, 1086
Granot, J., Miller, M., Piran, T., Suen, W. M., & Hughes, P. A. 2001, in GRBs in the Afterglow Era, ed. E. Costa, F. Frontera, & J. Hjorth (Berlin: Springer), 312
Granot, J., Nakar, E., & Piran, T. 2003, Nature, 426, 138
Granot, J., Panaitescu, A., Kumar, P., & Woosley, S. E. 2002, ApJ, 570, L61
Granot, J., Piran, T., & Sari, R. 1999, ApJ, 513, 679

Granot, J., Ramirez-Ruiz, E., & Perna, R. 2005, ApJ, 630, 1003
Granot, J., & Sari, R. 2002, ApJ, 568, 820
Guetta, D., Granot, J., & Begelman, M. C. 2005, ApJ, 622, 482
Huang, Y. F., Wu, X. F., Dai, Z. G., Ma, H. T., & Lu, T. 2004, ApJ, 605, 300
Kumar, P., & Granot, J. 2003, ApJ, 591, 1075
Kumar, P., & Panaitescu, A. 2000, ApJ, 541, L9
Lazzati, D., & Begelman, M. C. 2005, ApJ, 629, 903
Levinson, A., & Eichler, D. 2004, ApJ, 613, 1079
Lipkin, Y. M., et al. 2004, ApJ, 606, 381
Lipunov, V. M., Postnov, K. A., & Prokhorov, M. E. 2001, Astron. Rep., 45, 236
Moderski, R., Sikora, M., & Bulik, T. 2000, ApJ, 529, 151
Panaitescu, A., & Mészáros, P. 1999, ApJ, 526, 707
Pedersen, H., et al. 1998, ApJ, 496, 311
Peng, F., Königl, A., & Granot, J. 2005, ApJ, 626, 966
Ramirez-Ruiz, E., Celotti, A., & Rees, M. J. 2002, MNRAS, 337, 1349
Rhoads, J. E. 1997, ApJ, 487, L1
———. 1999, ApJ, 525, 737
Rossi, E., Lazzati, D., & Rees, M. J. 2002, MNRAS, 332, 945
Sari, R. 1997, ApJ, 489, L37
———. 1998, ApJ, 494, L49
Sari, R., & Piran, T. 1995, ApJ, 455, L143
Sari, R., Piran, T., & Halpern, J. 1999, ApJ, 519, L17
Sari, R., Piran, T., & Narayan, R. 1998, ApJ, 497, L17
Thompson, T. A. 2005, in Proc. 4th Workshop on Gamma-Ray Bursts in the Afterglow Era, in press (astro-ph/0504620)
Tominaga, N., et al. 2004, ApJ, 612, L105
van Paradijs, J., et al. 1997, Nature, 386, 686
Vlahakis, N., Peng, F., & Königl, A. 2003, ApJ, 594, L23
Wu, X. F., Dai, Z. G., Huang, Y. F., & Lu, T. 2005, MNRAS, 357, 1197
Zhang, B., Dai, X., Lloyd-Ronning, N. M., & Mészáros, P. 2004a, ApJ, 601, L119
Zhang, B., & Mészáros, P. 2002, ApJ, 571, 876
Zhang, W., Woosley, S. E., & Heger, A. 2004b, ApJ, 608, 365
Zhang, W., Woosley, S. E., & MacFadyen, A. I. 2003, ApJ, 586, 356